

Revision 1

Single-Crystal Elastic Properties of Minerals and Related Materials with Cubic Symmetry

Thomas S. Duffy

Department of Geosciences

Princeton University

Abstract

The single-crystal elastic moduli of minerals and related materials with cubic symmetry have been collected and evaluated. The compiled dataset covers measurements made over an approximately seventy year period and consists of 206 compositions. More than 80% of the database is comprised of silicates, oxides, and halides, and approximately 90% of the entries correspond to one of six crystal structures (garnet, rocksalt, spinel, perovskite, sphalerite, and fluorite). Primary data recorded are the composition of each material, its crystal structure, density, and the three independent nonzero adiabatic elastic moduli (C_{11} , C_{12} , and C_{44}). From these, a variety of additional elastic and acoustic properties are calculated and compiled, including polycrystalline aggregate elastic properties, sound velocities, and anisotropy factors. The database is used to evaluate trends in cubic mineral elasticity through consideration of normalized elastic moduli (Blackman diagrams) and the Cauchy pressure. The elastic anisotropy and auxetic behavior of these materials are also examined. Compilations of single-crystal elastic moduli provide a useful tool for investigation structure-property relationships of minerals.

Introduction

The elastic moduli are among the most fundamental and important properties of minerals (Anderson et al. 1968). They are central to understanding mechanical behavior and have applications across many disciplines of the geosciences. They control the stress-strain relationship under elastic loading and are relevant to understanding strength, hardness, brittle/ductile behavior, damage tolerance, and mechanical stability. Elastic moduli govern the propagation of elastic waves and hence are essential to the interpretation of seismic data, including seismic anisotropy in the crust and mantle (Bass et al. 2008; Mainprice 2015). As derivatives of the free energy, they are connected to a mineral's thermodynamic properties and are important for understanding equations of state, phase stability and the mechanism of phase transitions (Schreuer and Haussühl 2005b). They are related to quantities such as specific heat, Debye temperature, and the Grüneisen parameter. Elastic moduli provide fundamental insights into interatomic interactions, lattice dynamics, and the nature of bonding in crystals (Ledbetter 2000; Stixrude and Jeanloz 2015). Thus, there is a strong need for precise and accurate measurements of elastic moduli of many types of minerals.

Despite their utility, the full elastic tensors have been measured for only a small fraction of known minerals. Most of these measurements are at ambient pressure, and the knowledge of these properties at high pressures and/or variable temperatures is even more limited. This is primarily due to the stringent experimental requirements that must be met in order to characterize the full single-crystal elasticity tensor which requires determination of between 3 and 21 quantities depending on the mineral's crystal system.

Techniques for the measurement of elastic moduli have been developed and refined over more than a century. Early work in this area is summarized by Hearmon (Hearmon 1946) and Huntington (Huntington 1958). Beginning in the second half of the last century, the development and improvement of techniques based on propagation of ultrasonic pulses or measurement of resonant vibrational frequencies produced a large increase in the number and accuracy of elastic tensor measurements (for a historical review, see Li and Liebermann (2014)). The main experimental restriction in ultrasonic/resonant measurement techniques is the requirement for large high-quality single crystals. The development of laser-based Brillouin spectroscopy extended elasticity measurement techniques to transparent micro-crystals (Benedek and Fritsch 1966). The application of Brillouin scattering to geological materials first at ambient conditions (Weidner et al. 1975) and later at high pressures (Whitfield et al. 1976) has resulted in characterization of a number of geophysically important minerals, including high-pressure phases relevant to the Earth's mantle. There has also been recent development of further methods for single-crystal elasticity determination including gigahertz interferometry methods (Jacobsen et al. 2002) and synchrotron-based inelastic x-ray scattering (Hu et al. 2003). A number of review articles summarizing elasticity measurements and techniques are available (Schreuer and Haussühl 2005a; Bass 2007; Bass et al. 2008; Angel et al. 2009; Speziale et al. 2014).

In recent years, there has been an upsurge in the calculation of elastic moduli of minerals and other crystals by *ab initio* computer calculations using density functional theory. These calculations which are becoming increasingly routine can be applied to all types of materials. In addition, high-throughput methods have been used to develop a database of elastic properties of inorganic crystals consisting of more than 1000 inorganic compounds (de Jong et al. 2015). While complementary to experimental measurements, theoretical calculations have some limitations.

Uncertainties in individual elastic moduli are estimated to be ~10% or more for density functional approximations currently in use (Råsander and Moram 2015). Thus, there remains a strong need for experimental measurements as both a check on theoretical calculations and for achieving the highest precision in elasticity characterization.

Over the years, many compilations of experimental single-crystal elasticity data have been published (Hearmon 1946; Aleksandrov and Ryzhova 1961; Simmons and Wang 1971; Every and McCurdy 1992; Bass 1995; Isaak 2001). These generally provide only limited information, usually restricted to the elastic moduli themselves and possibly a few other parameters. These compilations are becoming increasingly out of date as new measurements accumulate. They are often not easily accessible in usable electronic form. Recently, there has been growing recognition of the need for reliable, accessible, and comprehensive databases of thermophysical properties of all types of materials (Hazen 2014). A number of databases of various mineral properties have been developed in recent years (Downs and Hall-Wallace 2003; Hacker and Abers 2004; Holland and Powell 2011; Lafuente et al. 2016; Rieder 2016).

In this work, a compilation of experimental measurements of the second-order adiabatic elastic moduli of minerals and related materials are reported. The dataset covers materials in the cubic crystal system at ambient conditions. In addition to the elastic moduli, a variety of related elastic and acoustic properties including polycrystalline aggregate properties and various anisotropy factors are also evaluated and tabulated. Such a dataset is useful in establishing structure-property relationships for minerals (Schreuer and Haussühl 2005b). A compilation of experimental single-crystal elastic properties can complement other thermodynamic and physical property databases as well.

Anisotropic Elasticity

The theory of elasticity of single crystals has been described extensively in the literature (Nye 1985; Every 2001; Schreuer and Haussühl 2005a; Stixrude and Jeanloz 2015) and only a brief summary is provided here. In the linear elastic region, the response of a solid to an external load is described by Hooke's Law which can be written as:

$$\sigma_{ij} = C_{ijkl} \epsilon_{kl}, \quad (1)$$

where σ_{ij} and ϵ_{kl} are components of the stress and strain tensors, and C_{ijkl} are the coefficients of the fourth-rank elastic stiffness tensor. Repeated indices are summed from one to three. As a result of the symmetry of the stress and strain tensors, Hooke's Law can be represented as a matrix equation:

$$\sigma_i = C_{ij} \epsilon_j. \quad (2)$$

Here we have used Voigt notation, reducing pairs of Cartesian integers to a single suffix and assuming summation of repeated indices from 1 to 6. The inverse relationship can be written:

$$\epsilon_i = S_{ij} \sigma_j, \quad (3)$$

where the S_{ij} are elements of the elastic compliance matrix, S , such that $S=C^{-1}$. The relationship between tensor and contracted quantities in Voigt notation is given elsewhere (Nye 1985).

The elastic stiffness matrix is symmetric and thus has 21 independent components in the most general case. The number of independent, nonzero stiffnesses will be further reduced depending on a material's crystal symmetry. In the case of cubic crystals, this reduces the numbers of required stiffness moduli to three as given below:

$$C = \begin{bmatrix} C_{11} & C_{12} & C_{12} & 0 & 0 & 0 \\ C_{12} & C_{11} & C_{12} & 0 & 0 & 0 \\ C_{12} & C_{12} & C_{11} & 0 & 0 & 0 \\ 0 & 0 & 0 & C_{44} & 0 & 0 \\ 0 & 0 & 0 & 0 & C_{44} & 0 \\ 0 & 0 & 0 & 0 & 0 & C_{44} \end{bmatrix}. \quad (4)$$

Elastic moduli depend on the conditions of measurement. The present database is a compilation of adiabatic elastic moduli. These arise from measurement techniques in which deformation is applied sufficiently quickly such that no energy exchange occurs between the sample and its environment. In contrast, when the deformation is applied slowly so the sample maintains thermal equilibrium with its surroundings, the isothermal moduli result. The adiabatic moduli are second derivatives of the internal energy with respect to strain whereas the isothermal moduli are the corresponding second derivatives of the Helmholtz free energy. The differences between adiabatic and isothermal moduli at ambient conditions are generally small, typically ~1-2%. Relationships between adiabatic and isothermal C_{ij} s and S_{ij} s for cubic crystals are provided in Davies (1974).

In the cubic system, the single-crystal elastic compliances, S_{ij} , are related to the stiffnesses, C_{ij} , through the following expressions:

$$S_{11} = \frac{C_{11} + C_{12}}{(C_{11} - C_{12})(C_{11} + 2C_{12})}, \quad (5)$$

$$S_{12} = \frac{-C_{12}}{(C_{11} - C_{12})(C_{11} + 2C_{12})}, \quad (6)$$

$$S_{44} = \frac{1}{C_{44}}. \quad (7)$$

The adiabatic elastic moduli are important for describing the propagation of acoustic waves. The wave equation for an anisotropic elastic solid is obtained by combining Hooke's Law with equations of motion of an elastic continuum. Considering long-wavelength plane wave solutions, one obtains a set of three linear equations:

$$(C_{ijkl}n_jn_l - \rho V^2 \delta_{ik})p_k = 0, \quad (8)$$

where C_{ijkl} are the elastic stiffnesses, the n_j are unit vectors of the wave propagation direction, and p_k are the polarization unit vectors. V is the acoustic velocity, and δ_{ik} is the Kronecker delta. This equation has non-trivial solutions that satisfy the Christoffel equation:

$$\det | C_{ijkl}n_jn_l - \rho V^2 \delta_{ik} | = 0. \quad (9)$$

Eqn. (9) has three solutions per each direction of \mathbf{n} which corresponds to three acoustic branches, one quasi-longitudinal and two quasi-shear. Piezoelectric effects occurring in acentric crystals produces additional, although generally small, effects on the velocity and attenuation of acoustic waves and the corresponding elastic moduli (Schreuer and Haussühl 2005a).

Individual elastic moduli may be identified with elastic waves propagating along certain directions or planes depending on crystal symmetry (Auld 1990). For cubic materials, C_{11} is the longitudinal modulus which governs propagation of compressional waves along the [100] direction. C_{44} is a shear modulus that governs a shear wave propagating in the (100) plane and polarized normal to it or a shear wave propagating along [110] and polarized along [001]. A second shear modulus given by $(C_{11}-C_{12})/2$ governs shear wave propagation along [110] and polarized along $[\bar{1}\bar{1}0]$. A full description of elastic waves in cubic crystals can be found in the literature (Auld 1990; Mainprice 2015).

Single-Crystal Elasticity Compilation

Due to the comparatively small number of coefficients needed to fully describe their elastic behavior, cubic minerals have been the subject of most intensive efforts to characterize their elasticity. The present database incorporates experimental single-crystal elasticity data at ambient conditions for 198 different compositions involving 477 individual measurements. The experimental data are supplemented by theoretical calculations for a few compounds (8) for which experimental data do not exist. The database covers measurements made over a ~70 year period (1947-present) with about 15% of the database representing studies reported in the last 25 years. While the database is focused on materials that are formally minerals, it also includes data on related non-mineral compositions (e.g., synthetic rare earth garnets as well as silicate garnets). This facilitates elucidation of compositional and structural trends. Approximately 2/3 of the database entries are recognized minerals. When multiple experimental studies exist, the elastic moduli are tabulated as unweighted arithmetic averages. In some cases there are clear outlier measurements which have been excluded. In other cases, existing measurements for a given material are inconsistent with each other and this has necessitated some judgement as to the likely correct values. Elasticity measurements pre-dating 1947 have been excluded as they have been largely superseded by later more accurate measurements.

The materials cataloged are grouped according to their Nickel-Strunz class (Table 1). About two-thirds of the database consists of silicates and oxides. Halides comprise an additional 21%, so that these three groups together comprise 87% of the database. A few crystal structure types also dominate the set of measurements (Table 2). 90% of the database entries belong to one of six crystal structures and a major portion of the dataset (72%) corresponds to measurements on

just three structures: garnet, rocksalt (B1-type), and spinel. While most structure types are restricted to just one or two of the mineral classes, the rocksalt, spinel, and sphalerite structures are found across at least four of the mineral classes. With the exception of diamond, native elements and intermetallics have not been included in the compilation at present. The elastic properties of cubic elements have been documented extensively in earlier databases (Simmons and Wang 1971; Every and McCurdy 1992) and systematic studies (Ledbetter 2000) and there are relatively few newer measurements on these materials.

Many other important properties of a mineral can be derived from its single-crystal elasticity tensor. The elastic properties of randomly oriented, isotropic, polycrystalline aggregates are of wide interest. The adiabatic or isentropic bulk modulus, K , describes the volume compression in response to hydrostatic pressure:

$$K = -V \left(\frac{dP}{dV} \right)_S, \quad (10)$$

where the subscript S refers to isentropic conditions. For a cubic crystal, the bulk modulus is rotationally invariant and is given by:

$$K = \frac{C_{11} + 2C_{12}}{3}. \quad (11)$$

Note that the ratio of the adiabatic bulk modulus to the isothermal bulk modulus measured at constant temperature is given by $1 + \alpha\gamma T$ where α is the thermal expansivity γ is the Gruneisen parameter, and T is temperature.

The shear modulus is determined by the ratio of shear stress to shear strain. In crystalline solids, the shear modulus varies with direction. Bounds on the effective shear modulus, G , of a randomly oriented polycrystalline aggregate may be obtained through statistical elasticity models that provide averages over all directions (Watt 1988). The Voigt and Reuss bounds, based on assumptions of strain and stress continuity, respectively, provide upper and lower limits on the average shear modulus. For cubic symmetry, these are calculated using:

$$G_V = \frac{1}{5}(C_{11} - C_{12} + 3C_{44}), \quad (12)$$

$$G_R = \frac{5}{(4S_{11} - 4S_{12} + 3S_{44})} = \frac{5(C_{11} - C_{12})C_{44}}{4C_{44} + 3(C_{11} - C_{12})}, \quad (13)$$

where G_V and G_R are the Voigt and Reuss bounds on the shear modulus, respectively.

The arithmetic average of the Voigt and Reuss bounds, known as the Voigt-Reuss-Hill (VRH) average, G , is given by:

$$G = \frac{G_V + G_R}{2}. \quad (14)$$

Although it lacks theoretical justification, there is good agreement between the VRH shear modulus calculated from single-crystal elasticity data and direct measurements on isotropic polycrystals (Watt et al. 1976). In general, however, the appropriate shear modulus may depend on the nature of grain-to-grain interactions in an aggregate. A number of other bounding schemes are also available, and the narrower Hashin-Shtrikman bounds (G_{HS1} , G_{HS2}) are tabulated using expressions of (Brown 2015). The arithmetic average of the Hashin-Shtrikman bounds (G_{HSA}) is also provided in the compilation.

Young's modulus (E) and Poisson's ratio (ν) are important elastic parameters of a material.

Expressions for the variation of these quantities with direction in a cubic crystal are provided in (Ting and Chen 2005; Paszkiewicz and Wolski 2007). Isotropic polycrystalline aggregate values for E and ν are obtained from the bulk modulus and aggregate (VRH) shear modulus using:

$$\nu = \frac{3K - 2G}{2(3K + G)}, \quad (15)$$

and

$$E = \frac{9GK}{(G + 3K)}. \quad (16)$$

The elastic wave velocities for an isotropic aggregate are given by:

$$V_P = \sqrt{\frac{K + \frac{4}{3}G}{\rho}}, \quad V_B = \sqrt{\frac{K}{\rho}}, \quad V_S = \sqrt{\frac{G}{\rho}}, \quad (17)$$

where V_P , V_B , and V_S are the compressional, bulk, and shear sound velocities, respectively, and ρ is the density.

The ratio of compressional to shear velocity, V_P/V_S , is often useful as a compositional diagnostic in interpreting seismic data. This is given by:

$$\frac{V_P}{V_S} = \frac{K}{G} + \frac{4}{3}. \quad (18)$$

Elastic anisotropy is an important aspect of the mechanical behavior of crystals (Ledbetter and Migliori 2006). Traditionally, the elastic anisotropy of cubic crystals was expressed using the Zener anisotropy factor, A^Z (Zener 1948):

$$A^Z = \frac{2C_{44}}{C_{11} - C_{12}}. \quad (19)$$

which is the ratio of the ratio of the two limiting values of the shear modulus, C_{44} and $(C_{11}-C_{12})/2$. An elastically isotropic material has $A^Z=1$ and anisotropic materials are characterized by either A^Z greater than or less than one depending of the relative magnitudes of the two extrema in shear moduli.

Chung and Buessem (1967) showed that the difference between the Voigt and Reuss bounds on the shear modulus of a cubic crystal provides an alternative measure of the elastic anisotropy, A^G :

$$A^G = \frac{G_V - G_R}{G_V + G_R} = \frac{3(A^Z - 1)^2}{3(A^Z - 1)^2 + 25A^Z}. \quad (20)$$

In terms of the individual C_{ij} s, A^G can be written:

$$A^G = \frac{3[(C_{11} - C_{12}) - 2C_{44}]^2}{12C_{44}^2 + 38C_{44}(C_{11} - C_{12}) + 3(C_{11} - C_{12})^2}. \quad (21)$$

This measure, usually expressed as a percentage, has the advantage that its takes a value of zero for an isotropic material and allows for more direct quantitative comparison of anisotropy magnitudes among crystals.

Recently there has been renewed interest in metrics for characterizing the elastic anisotropy of crystals (Ledbetter and Migliori 2006; Ranganathan and Ostoja-Starzewski 2008; Kube 2016; Kube and de Jong 2016). The new measures extend earlier approaches by taking into account all the individual components of the elasticity tensor including both bulk and shear contributions. They also can be applied to all crystal systems. The “universal” elastic anisotropy index, A^U , is defined as (Ranganathan and Ostoja-Starzewski 2008):

$$A^U = 5 \frac{G_V}{G_R} + \frac{K_V}{K_R} - 6, \quad (22)$$

which, for the cubic case, reduces to:

$$A^U = 5 \frac{G_V}{G_R} - 5. \quad (23)$$

Alternatively, a universal log-Euclidean anisotropy index has been proposed and is defined as (Kube 2016):

$$A^L = \sqrt{\left[\ln \left(\frac{K_V}{K_R} \right) \right]^2 + 5 \left[\ln \left(\frac{G_V}{G_R} \right) \right]^2}, \quad (24)$$

where K_V and K_R are the Voigt and Reuss bounds on the bulk modulus which are equivalent for cubic crystals but not for other symmetries. As a result, for cubic minerals, this simplifies to:

$$A^L = \sqrt{5} \ln \left(\frac{G_V}{G_R} \right). \quad (25)$$

These latter two anisotropy indices (Eqns. 23 and 24) can be related to measures of the distance between different orientational averages of the modulus and compliance tensors (Kube 2016).

Their universal nature, incorporation of both bulk and shear components of anisotropy, and zero value for the isotropic case are advantages for these approaches in describing elastic anisotropy.

The orientation-dependent Poisson's ratio, $\nu(\mathbf{n}, \mathbf{m})$ requires the specification of two directions: lateral contraction/extension in one direction (\mathbf{n}) and the corresponding extension/contraction in a normal direction (\mathbf{m}). Baughman et al. (1998) have shown that with very few exceptions the extreme values of Poisson's ratio for a cubic crystal occur for the case of strain along $\langle 110 \rangle$ and the corresponding orthogonal strain along $\langle 001 \rangle$ and $\langle 1\bar{1}0 \rangle$. The value of Poisson's ratio in these directions can be expressed as (Baughman et al. 1998):

$$\nu(110, 001) = \frac{4C_{12}C_{44}}{2C_{11}C_{44} + (C_{11} - C_{12})(C_{11} + 2C_{12})} = \frac{2A^Z C_{12}}{3K + A^Z C_{11}}, \quad (26)$$

and

$$\nu(110,1\bar{1}0) = \frac{2C_{11}C_{44} - (C_{11} - C_{12})(C_{11} + 2C_{12})}{2C_{11}C_{44} + (C_{11} - C_{12})(C_{11} + 2C_{12})} = \frac{3K - A^Z C_{11}}{3K + A^Z C_{11}}. \quad (27)$$

The compiled elastic moduli and quantities derived from them are described in Table 3 and contained in a Microsoft Excel spreadsheet included as supplementary material. The record for each entry includes its composition, structure, density, and the three elastic stiffness components (C_{11} , C_{12} , and C_{44}). In addition to the density and C_{ij} s, the reduced adiabatic elastic moduli (C_{12}/C_{11} , C_{44}/C_{11}), adiabatic elastic compliances (Eqns. 5-7), aggregate elastic moduli (Eqns. 11-16), acoustic velocities (Eqns. 17-18), anisotropy factors (Eqns. 19-25), and extreme values of Poisson's ratio (Eqns. 26-27) have been calculated and included in the compilation.

Results

Cubic Elasticity Systematics: Blackman diagrams

For cubic materials, plots of the reduced elastic stiffnesses, C_{12}/C_{11} against C_{44}/C_{11} , known as Blackman diagrams, are useful for identifying trends and interrelationships in mechanical and bonding properties (Blackman 1938; Ledbetter 2000; Ledbetter and Migliori 2008). The Blackman plot of Figure 1 highlights the general features of this type of representation. Poisson's ratio, ν , is an indicator of interatomic bonding character and a fundamental metric for a material's mechanical response (Greaves et al. 2011; Ji et al. 2018). Constant values of the aggregate Poisson's ratio are plotted as red dotted lines in Fig. 1. Lower values of ν plot in the lower right-hand side of the plot and increase upward and to the right. The dotted blue lines emanating from the upper left of the diagram give values of the Zener anisotropy ratio, A^Z , with the heavier blue line indicating the

condition for elastic isotropy ($A^Z=1$). The left and top edges of the diagram define two of the three Born stability limits for a cubic crystal:

$$C_{11} > |C_{12}|, \quad C_{44} > 0. \quad (28)$$

Also shown in the diagram is a dashed black line corresponding to the Cauchy relation:

$$C_{12} = C_{44}. \quad (29)$$

This is a fundamental and historically important result that arises in the case of a central force pair potential. It reflects the nature of bonding at the atomic level. The C_{ij} s of ionically bonded materials generally approach the Cauchy relationship. Materials which fall above the Cauchy line ($C_{12} > C_{44}$) are described as having a positive Cauchy pressure whereas materials below it ($C_{44} > C_{12}$) have a negative Cauchy pressure. A negative Cauchy pressure requires angular corrections and hence more covalent bonding character. A positive Cauchy pressure necessitates accounting for many-body interactions and hence a higher portion of metallic bonding.

Previously, Blackman diagrams have been used to describe elements and binary compounds (Ledbetter 2000; Ledbetter and Migliori 2008). Here we apply this approach to the wider range of compositions and structures found in cubic minerals. Figure 1 shows a plot of reduced elastic moduli for the compiled compounds. Clear groupings in terms of composition and structure type are immediately visible. In general, there is a tendency for minerals to cluster around three major trends. Two of these are defined by the lines representing elastic isotropy ($A^Z=1$, thick dashed blue line) and the Cauchy relationship ($C_{12} = C_{44}$, dashed black line). Note that the intersection of the Zener isotropy and the Cauchy relationship implies the interrelationship: $C_{11} = 3C_{12} = 3C_{44}$. The third trend follows a line given by (green line in Fig. 1):

$$C_{11} = \frac{2}{3}(C_{12} + 2C_{44}). \quad (30)$$

This latter relationship has been identified empirically as associated with covalent compounds (Ledbetter 2000).

Silicates, dominantly garnets and spinels, tend to cluster near the intersection of the lines defining elasticity isotropy and the Cauchy relationship. Oxides are more diverse with garnets, rocksalts, and spinels falling into distinct bands of similar anisotropy but covering a range of Poisson's ratios. Most oxides exhibit a positive Cauchy pressure. Halides often trend along the Cauchy relation reflecting dominant ionic bonding for many of these but with a subset also following the relationship defined by Eqn (30). In general, the vast majority of minerals exhibit either a positive Cauchy pressure or a weakly negative one. Strong negative Cauchy pressure corresponding to low values of Poisson's ratio are mostly restricted to a few compounds including diamond, pyrite, cubic Si_3N_4 , and qingsongite (BN).

Figure 2 shows a Blackman plot for the subset of materials in the garnet and spinel structures which together make up about 50% of the database. The AB_2O_4 spinel compounds may be classified according to their B cation. Al-bearing spinels have large anisotropy with A^Z typically in the range of 2.3-2.5. The anisotropy of hercynite, FeAl_2O_4 , is somewhat of anomalous ($A^Z=3.1$) compared to other aluminate spinels including those with other transition elements in the A site. It has been noted that for this material the bulk modulus from single-crystal elasticity measurements (Wang and Simmons 1972) differs significantly from that found from pressure-volume static compression data (after correcting for differences between adiabatic and isothermal moduli) (Nestola et al. 2015).

Ferrite spinels define a separate trend that span a range of anisotropies ($A^Z=1.1$ to 2.2) but only a limited range of Poisson's ratio around $\nu=0.33$. They tend to have a similar C_{12}/C_{11} ratio but widely varying C_{44}/C_{11} values. The chromite spinels, on the other hand, show wide variability

in C_{12}/C_{11} but with little variation in C_{44}/C_{11} . The wide span of C_{12}/C_{11} extending to values approaching unity reflects elastic softening of the tetragonal shear modulus, $(C_{11}-C_{12})/2$ due to proximity to a tetragonal distortion occurring below room temperature in several of these materials as a result of a cooperative Jahn-Teller effect (Kino et al. 1972). The elastic properties of ulvöspinel, Fe_2TiO_4 , also reflect softening associated with a Jahn-Teller driven phase transition (Syono et al. 1971). Silicate spinels, mostly $(\text{Mg,Fe})_2\text{SiO}_4$ ringwoodites (both anhydrous and hydrous), have low anisotropies and Poisson's ratio compared with other spinels.

Garnets are an important group of minerals with both geophysical and technical applications. Despite the complexity of the garnet structure and associated chemical variability across the dodecahedral, octahedral, and tetrahedral sites, both silicate and oxide garnets fall in a restricted field in a Blackman diagram. Within this limited space, however, clear compositional trends can be identified as seen in Figure 3 and Table 4. Among silicate garnets, members of the pyralspite group (pyrope, almandine, and spessartine), $(\text{Mg,Fe,Mn})_3\text{Al}_2\text{Si}_3\text{O}_{12}$, all are found in the same narrow range with reduced elastic moduli $C_{12}/C_{11}=0.364(4)$ and $C_{44}/C_{11}=0.311(3)$, where the numbers in parentheses are one standard deviation from the average. The corresponding values of Poisson's ratio also adopt a narrow range from 0.266 to 0.274 while the Zener anisotropy values all lie between 0.96 and 0.99. Grossular-rich garnets exhibit a higher degree of anisotropy ($A^Z=0.91(2)$) and lower values of C_{12} and Poisson's ratio ($\nu=0.241(6)$). For garnets with Cr^{3+} and Fe^{3+} in the octahedral site (andradite, uvarovite) the anisotropy factor further increases ($A^Z=0.83(3)$) while Poisson's ratio is 0.259(1). Overall, clear compositional trends are evident for substitution of divalent cations in the dodecahedral site, trivalent cations in the octahedral site, and the hydrogrossular substitution ($4\text{H}^+ \rightarrow \text{Si}^{4+}$) in the tetrahedral site (Figure 3). The latter substitution is associated with both a decrease in Poisson's ratio and Zener anisotropy.

Compositions in the pyrope-majorite solid solution differ only slightly from pyralspite garnets with higher values of C_{12}/C_{11} and even lower anisotropy. A Na-rich majorite, however, is distinctly different from the other silicate garnets.

The general chemical formula for rare earth oxide garnets can be written: $RE_3Y_2Z_3O_{12}$, where the dodecahedral site is occupied by a rare earth (RE) cation and the octahedral and tetrahedral sites (Y and Z) are typically aluminum, iron, or gallium. Due to their important technological properties, the elastic tensors of a number of RE-garnet compositions have been measured and 21 such compositions are included in this database. The rare-earth oxide garnets show minor but distinct differences from the silicate garnets. The elastic behavior of these garnets varies systematically with the octahedral/tetrahedral cation showing distinct groupings for aluminum, gallium, and iron garnets (Figure 3). These garnets also have low elastic anisotropy but in contrast to the silicates, A^Z is generally slightly greater than 1. The main change exhibited by RE-garnets is that Poisson's ratio increases from the aluminate ($\nu=0.250(4)$) to gallate ($\nu=0.280(5)$) to ferrite ($\nu=0.293(19)$) garnets as C_{12}/C_{11} increases and C_{44}/C_{11} decreases across this sequence. RE-Fe garnets show the largest spread in values of reduced moduli. Among the RE-iron garnets, $Tb_3Fe_5O_{12}$, appears to be an outlier compared to trends for other garnets. Other systematic relationships involving garnet elasticity including dependence of elastic moduli on lattice parameter as well as velocity-density systematics have been explored elsewhere (Babuska et al. 1978; Kitaeva et al. 1985; Bass 1986).

A Blackman diagram for binary compounds in the rocksalt (B1), cesium chloride (B2), and sphalerite (B3) structures is shown in Figure 4. While there are only a few compounds in the B2 structure, the rocksalt and sphalerite structures combine to make up about 30% of the database. A number of details in the trends in these compounds have been discussed elsewhere (Ledbetter

2000). Most of the rocksalt and CsCl halides follow closely to Cauchy relationship reflecting the dominance of ionic bonding. Sphalerite-structured compounds reflect a higher degree of covalent bonding and follow the trend of Eqn. (30) for halides, sulfides, as well as the single representative of each of the carbide, nitride, and phosphide classes. Compositions along the (Mg,Fe)O solid solution show strong changes in Poisson's ratio and Zener anisotropy with values extending from (0.18, 1.5) for periclase (MgO) to (0.36, 0.96) for wüstite (Fe_{0.95}O). The trend for Mg-Fe substitution lies close to the values adopted by other transition element monoxides (MnO, CoO, CdO). On the other hand, the alkaline earth oxides (MgO, CaO, SrO, and BaO) define a separate trend in which the anisotropy changes strongly with cation radius but Poisson's ratio does not, although the behavior of BaO deviates from the others. The differences in Cauchy behavior of B1 oxides have been discussed previously (Weidner et al. 1982).

Cauchy Pressure

Figure 5 shows the shear/bulk modulus ratio plotted against the Cauchy pressure ($C_{12}-C_{44}$). The different structures types define three distinct linear trends in Fig. 5. One such trend is exhibited primarily by silicate and oxides minerals whereas the halides and sulfides (and nitrides) define a second, steeper trend. A small number of compositions possess larger G/K values and large negative Cauchy pressure: diamond, qingsongite (c-BN), cubic silicon nitride, SiC, and MgO. These define a third linear trend, shallower than the other two (Figure 5, inset). The different slopes of the three relationships largely reflect differences in compressibility between mineral classes. Both positive Cauchy pressure and larger G/K value are associated with greater hardness

and more brittle behavior whereas smaller values for both quantities are associated more ductile behavior, consistent with general bonding trends (Pettifor 1992; Niu et al. 2012).

Elastic Anisotropy

In order to illustrate compositional and structural variations in elastic anisotropy of cubic minerals, the Zener anisotropy ratio, A^Z , is plotted against Kube's Log-Euclidean Anisotropy Index, A^L in Figure 6. The relationship between the two anisotropy measures is the following:

$$A^L = \sqrt{5} \ln \left(\frac{6A^Z + 6 / A^Z + 13}{25} \right). \quad (31)$$

Zener anisotropies of 1, 2, and 3 (or 1, 0.5, 0.333), for example, correspond to A^L values of 0, 0.25, and 0.62, respectively. The A^L values for the cubic dataset are within the range of 0 and 1 with the exception of NiCr_2O_4 spinel which shows extremely large anisotropy ($A^Z=23.2$, $A^L = 4.0$).

A variety of structural trends in anisotropy are evident in Figure 6. For materials with $A^Z < 1$, the B1 (rocksalt) halides generally exhibit among the highest anisotropy values. The anisotropy of these compounds scales with both cation ($\text{Rb} > \text{K} > \text{Na}$) and anion ($\text{I} > \text{Br} > \text{Cl} > \text{F}$) size. The Li halides (LiX , $\text{X}=\text{F}$, Cl , Br , I) show distinctly different behavior with the opposite orientation of anisotropy ($A^Z > 1$) and little dependence of anisotropy on anion size. The behavior of these latter compounds has been attributed to the small size of the Li cation and the corresponding importance of anion repulsion effects (Ledbetter 2000). Distinct groupings can also be observed for other compositional/mineral groups with $A^Z < 1$ including oxide fluorites, halide perovskites, and silicate garnets.

For compounds with $A^Z > 1$, a variety of structures and classes are represented among those with the highest anisotropy including Cu sphalerites, nitrates, and some oxide spinels. Overall, the oxide spinels span a wide range of anisotropy values with the largest anisotropies in the aluminate spinels (spinel-hercynite) as well as ulvöspinel, FeTi_2O_4 , and NiCr_2O_4 . The oxide rocksalts exhibit modest range of anisotropy ($A^L < 0.13$) whereas the oxide garnets are nearly isotropic ($A^L < 0.005$) as discussed above.

Auxetic Behavior

Poisson's ratio is determined by the ratio of the lateral extension/contraction in one direction to the corresponding compression/extension in a normal direction. In most cases, Poisson's ratio is positive such that an axial compression produces a lateral expansion and vice versa. Materials exhibiting a negative Poisson's ratio in which an axial compression produces a lateral contraction for one or more directions are known as auxetic. There has been much recent interest in identifying and understanding auxetic behavior in both natural and synthetic materials (Baughman et al. 1998; Paszkiewicz and Wolski 2007; Lethbridge et al. 2010). A material with a negative bulk Poisson's ratio is known as fully auxetic and only one such natural material is known (cristobalite (Yeganeh-Haeri et al. 1992)). Materials with negative Poisson's ratios in certain combinations of directions are known as partially auxetic.

Previous studies have shown that the maximum and minimum values of Poisson's ratio for cubic materials generally occur in specific directions (Eqns. 26 and 27). Furthermore, it is known that partially auxetic behavior is commonly observed in cubic metals and intermetallic compounds (Baughman et al. 1998; Wang et al. 2012). The magnitude of the extrema in Poisson's ratio are correlated to the elastic anisotropy (Lethbridge et al. 2010; Wang et al. 2012). Figure 7 illustrates

this relationship for the mineral elasticity dataset. For materials with $A^Z < 1$, the maximum in Poisson's ratio occurs along $\nu(110, 1\bar{1}0)$ and the minimum $\nu(\mathbf{n}, \mathbf{m})$ value occurs for $\nu(110, 001)$ with values that approach zero but remain positive. For materials with $A^Z > 1$, the opposite relationship holds with $\nu(110, 001)$ and $\nu(110, 1\bar{1}0)$ yielding the maximum and minimum Poisson's ratios, respectively. According to Eqns. (26) and (27), $\nu(110, 001)$ should always be positive (as long as $C_{12} > 0$), so auxetic behavior is not expected in this direction. On the other hand, $\nu(110, 1\bar{1}0)$ will be negative when $3K > A^Z C_{11}$ (Jain and Verma 1990).

In general, partially auxetic behavior is found for materials with both $A^Z > 1$ (Fig. 6) and large elastic anisotropy (Figs. 1, 6, and 7). A negative Poisson's ratio can occur for lower anisotropy materials if C_{44}/C_{11} is relatively large (e.g. qingsongite, BN, $A^Z=1.5$, $A^L=0.09$) but generally is found for materials with $A^Z > 2$ ($A^L > 0.25$) (Figs. 1, 6, 7). Partially auxetic behavior occurs for several types of materials including oxide spinels, pyrite-structured nitrates (nitrobarite, $\text{Ba}(\text{NO}_3)_2$ and lead nitrate, $\text{Pb}(\text{NO}_3)_2$), and halides and sulfides with the sphalerite structure (Figs. 1, 7). Among the spinels, partially auxetic behavior occurs for aluminate spinels including the minerals spinel (MgAl_2O_4), hercynite (FeAl_2O_4), galaxite (MnAl_2O_4), and gahnite (ZnAl_2O_4) but generally does not occur in other spinels (with the exception of $(\text{Ni}, \text{Zn})\text{Cr}_2\text{O}_4$ and ulvöspinel, FeTi_2O_4 (Fig. 2)). The B1 Li-halides exhibit values of $\nu(110, 1\bar{1}0)$ that approach zero but only griceite (LiF) is partially auxetic.

Materials which satisfy Eqn. (30) also tend to be partially auxetic (Fig. 1). Among the B3 sphalerite compounds that exhibit negative Poisson's ratio include a nitride (qingsongite, BN), a carbide (moissanite, SiC), copper halides (nantokite, CuCl and marshite, CuI) and various members of the sulfide class including selenides and tellurides (metacinnabar, $\beta\text{-HgS}$, sphalerite, ZnS, coloradoite, HgTe, Tiemannite, HgSe, and stilleite, ZnSe). Based on theoretical calculations,

it was reported that a large number of binary intermetallics in the CsCl (B2) structure exhibit negative values of Poisson's ratio for $\nu(110,1\bar{1}0)$ (Wang et al. 2012). The present dataset contains only a few B2 compounds (Cs halides and salammoniac, NH_4Cl). All of these compounds have $A^Z < 1$ and thus do not exhibit partially auxetic behavior.

Implications

Measurement of single-crystal elastic moduli in cubic crystals provide a direct determination of the bulk modulus. However, most laboratory determinations of the bulk modulus are made less directly by fitting an equation of state such as the Birch-Murnaghan equation to volume compression data, usually obtained by x-ray diffraction (Duffy and Wang 1998; Angel 2000). Comparison of bulk moduli from ambient-pressure elasticity measurements and volume compression data (with appropriate corrections for different thermodynamic conditions) are an important means to cross-check and validate different measurements. Combination of elasticity measurements of the ambient bulk modulus K with volume compression data avoids inherent covariance between fit values of the bulk modulus and its pressure derivative, $K' = (dK/dP)$, enabling tighter constraints to be placed on the latter quantity (Bass et al. 1981). The present data compilation can serve as a convenient resource for comparison and cross-checks with static compression (Angel 2000) or sound velocity data on polycrystalline samples (Wang and Ji 2001; Li and Liebermann 2014).

The dataset may also be used to identify materials for which elasticity data may be questionable due either to large differences between independent measurements or deviations from trends among related compositions or structures (Sirdeshmukh and Subhadra 2005). Outliers might

also reflect some unusual feature of a given mineral's elasticity. As one example, ulvöspinel, Fe_2TiO_4 , has been reported to have anomalously low elastic moduli compared with other spinels (Syono et al. 1971). The low value of $C_{11}-C_{12}$ is attributed to elastic softening associated with a cooperative Jahn-Teller structural distortion below room temperature. Notably, all the individual elastic moduli are rather low for this material. The resulting aggregate bulk and shear moduli (Hill averages) for ulvöspinel are 122 GPa and 26 GPa, respectively, again considerably lower than trends based on other spinels. Diamond anvil cell static compression determinations of the isothermal bulk modulus for Fe_2TiO_4 produce larger, but divergent, results with one study reporting a bulk modulus of 147 GPa (Xiong et al. 2014) while another study reported a K value of 251 GPa (Yamanaka et al. 2009), with K' fixed to 4 in both cases. While spinels may exhibit cation disorder in the octahedral and tetrahedral sites (Hazen and Yang 2015), these are unlikely to fully explain the large differences between studies observed here. Given the divergence between static compression and ultrasonic elasticity, it is not possible to draw firm conclusions about ulvöspinel elastic properties at present, and re-measurement of the elastic moduli of this material may be warranted.

Single-crystal elasticity data are also useful as input to computer codes, many developed in just the last few years, available for calculation and 2D or 3D visualization of anisotropic elastic and acoustic properties (Mainprice 1990; Marmier et al. 2010; Mainprice et al. 2011; Walker and Wookey 2012; Gaillac et al. 2016; Jaeken and Cottenier 2016; Muñoz-Santiburcio and Hernández-Laguna 2017). In geophysics, there is particular interest in programs for determining seismic anisotropy and the elastic properties of textured rocks (Mainprice et al. 2011; Walker and Wookey 2012). Elasticity data are also required in various computations including thermodynamic modeling of phases at high pressures and temperatures (Holland and Powell 2011).

Finally, the elasticity compilation can be used to further probe systematic relationships among elastic and acoustic properties and structural parameters in mineral groups which have been a subject of long interest in mineral physics (Anderson et al. 1968; Reichmann et al. 2013; Bruschini et al. 2015). A number of future extensions of this database are possible most obviously inclusion of non-cubic minerals. Incorporation of pressure and temperature dependencies of elastic moduli and theoretical calculations are also of interest.

Acknowledgements

Robert Liebermann provided helpful comments and historical context and David Teter shared his unpublished elasticity compilation. This work benefitted from fruitful discussions with Sergio Speziale and Ilias Zouboulis.

References

- Aleksandrov, K.S., and Ryzhova, T.V. (1961) The elastic properties of crystals. *Sov. Phys. Cryst.*, 6, 228–252.
- Anderson, O., Schreiber, E., and Liebermann, R. (1968) Some elastic constant data on minerals relevant to geophysics. *Reviews of Geophysics*, 6, 491-.
- Angel, R. (2000) Equations of state. *Rev. Mineral. Geochem.*, 41, 35–59.
- Angel, R., Jackson, J., Reichmann, H., and Speziale, S. (2009) Elasticity measurements on minerals: A review. *European Journal of Mineralogy*, 21, 525–550.
- Ardell, A.J. (2017) The roles of auxeticity and volume fraction on γ' precipitate microstructures in nickel-base alloys. *Philosophical Magazine Letters*, 97, 35–42.
- Auld, B.A. (1990) *Acoustic Fields and Waves in Solids*, 2nd ed., 435 p. Krieger, Malabar, FL.

- Babuska, V., Fiala, J., Kumazawa, M., Ohno, I., and Sumino, Y. (1978) Elastic properties of garnet solid-solution series. *Physics of the Earth and Planetary Interiors*, 16, 157–176.
- Bass, J.D. (1986) Elasticity of uvarovite and andradite garnets. *Journal of Geophysical Research: Solid Earth*, 91, 7505–7516.
- (1995) Elasticity of minerals, glasses, and melts. In T.J. Ahrens, Ed., *Mineral Physics & Crystallography: A Handbook of Physical Constants* pp. 45–63. American Geophysical Union, Washington DC.
- Bass, J.D. (2007) Theory and practice -- Techniques for measuring high P/T elasticity. In G.D. Price, Ed., *Treatise on Geophysics*, Vol. 2 Mineral Physics pp. 269–295. Elsevier, New York.
- Bass, J.D., Liebermann, R.C., Weidner, D.J., and Finch, S.J. (1981) Elastic properties from acoustic and volume compression experiments. *Physics of the Earth and Planetary Interiors*, 25, 140–158.
- Bass, J.D., Sinogeikin, S.V., and Li, B. (2008) Elastic properties of minerals: A key for understanding the composition and temperature of Earth's interior. *Elements*, 4, 165–170.
- Baughman, R.H., Shacklette, J.M., Zakhidov, A.A., and Stafström, S. (1998) Negative Poisson's ratios as a common feature of cubic metals. *Nature*, 392, 362–365.
- Benedek, G.B., and Fritsch, K. (1966) Brillouin scattering in cubic crystals. *Physical Review*, 149, 647–662.
- Blackman, M. (1938) On anomalous vibrational spectra. *Proceedings of the Royal Society of London Series A*, 164, 62–79.
- Brown, J.M. (2015) Determination of Hashin-Shtrikman bounds on the isotropic effective elastic moduli of polycrystals of any symmetry. *Computers & Geosciences*, 80, 95–99.
- Bruschini, E., Speziale, S., Andreozzi, G.B., Bosi, F., and Hålenius, U. (2015) The elasticity of MgAl₂O₄–MnAl₂O₄ spinels by Brillouin scattering and an empirical approach for bulk modulus prediction. *American Mineralogist*, 100, 644–651.
- Chung, D.H., and Buessem, W.R. (1967) The Elastic Anisotropy of Crystals. *Journal of Applied Physics*, 38, 2010–2012.
- Davies, G. (1974) Effective elastic-moduli under hydrostatic stress .1. Quasi-harmonic theory. *Journal of Physics and Chemistry of Solids*, 35, 1513–1520.
- de Jong, M., Chen, W., Angsten, T., Jain, A., Notestine, R., Gamst, A., Sluiter, M., Ande, C.K., Zwaag, S. van der, Plata, J.J., and others (2015) Charting the complete elastic properties of inorganic crystalline compounds. *Scientific Data*, 2, sdata20159.

- Downs, R.T., and Hall-Wallace, M. (2003) The American Mineralogist crystal structure database. *American Mineralogist*, 88, 247–250.
- Duffy, T.S., and Wang, Y.B. (1998) Pressure-volume-temperature equations of state. (R.J. Hemley, Ed.) *Rev. Mineral. Geochem.*, 37, 425–457.
- Every, A.G. (2001) The elastic properties of solids: Static and dynamic principles. In M. Levy, H. Bass, and R. Stern, Eds., *Handbook of Elastic Properties of Solids, Liquids and Gases* Vol. 1, pp. 3–36. Elsevier, New York.
- Every, A.G., and McCurdy, A.K. (1992) Second and higher order elastic constants. In D.F. Nelson, Ed., *Landolt-Börnstein Tables* Vol. III/29a, pp. 1–743. Springer-Verlag, Berlin.
- Gaillac, R., Pullumbi, P., and Coudert, F.-X. (2016) ELATE: an open-source online application for analysis and visualization of elastic tensors. *Journal of Physics: Condensed Matter*, 28, 275201.
- Greaves, G.N., Greer, A.L., Lakes, R.S., and Rouxel, T. (2011) Poisson's ratio and modern materials. *Nature Materials*, 10, 823–37.
- Hacker, B.R., and Abers, G.A. (2004) Subduction Factory 3: An Excel worksheet and macro for calculating the densities, seismic wave speeds, and H₂O contents of minerals and rocks at pressure and temperature. *Geochemistry Geophysics Geosystems*, 5, Q01005.
- Hazen, R.M. (2014) Data-driven abductive discovery in mineralogy. *American Mineralogist*, 99, 2165–2170.
- Hazen, R.M., and Yang, H. (2015) Effects of cation substitution and order-disorder on P-V-T equations of state of cubic spinels. *American Mineralogist*, 84, 1956–1960.
- Hearmon, R.F.S. (1946) The elastic constants of anisotropic materials. *Reviews of Modern Physics*, 18, 409–440.
- Holland, T., and Powell, R. (2011) An improved and extended internally consistent thermodynamic dataset for phases of petrological interest, involving a new equation of state for solids. *Journal of Metamorphic Geology*, 29, 333–383.
- Hu, M.Y., Sturhahn, W., Toellner, T.S., Mannheim, P.D., E. Brown, D., Zhao, J., and Alp, E.E. (2003) Measuring velocity of sound with nuclear resonant inelastic x-ray scattering. *Physical Review B*, 67, 094304.
- Huntington, H.B. (1958) The Elastic constants of crystals. *Solid State Physics*, 7, 213–351.
- Isaak, D.G. (2001) Elastic properties of minerals and planetary objects. In M. Levy, H. Bass, and R. Stern, Eds., *Handbook of Elastic Properties of Solids, Liquids, and Gases*, Vol. III, pp. 325–376. Academic, New York.

- Jacobsen, S.D., Reichmann, H.-J., Spetzler, H.A., Mackwell, S.J., Smyth, J.R., Angel, R.J., and McCammon, C.A. (2002) Structure and elasticity of single-crystal (Mg,Fe)O and a new method of generating shear waves for gigahertz ultrasonic interferometry. *Journal of Geophysical Research: Solid Earth*, 107, 2037.
- Jaeken, J.W., and Cottenier, S. (2016) Solving the Christoffel equation: Phase and group velocities. *Computer Physics Communications*, 207, 445–451.
- Jain, M., and Verma, M.P. (1990) Poisson ratios in cubic crystals corresponding to (110) loading. *Indian Journal of Pure & Applied Physics*, 28, 178–182.
- Ji, S., Li, L., Motra, H.B., Wuttke, F., Sun, S., Michibayashi, K., and Salisbury, M.H. (2018) Poisson's ratio and auxetic properties of natural rocks. *Journal of Geophysical Research: Solid Earth*, 2017JB014606.
- Kino, Y., Mullen, M., and Luthi, B. (1972) Cooperative Jahn-Teller Phase-Transition in Nickel-Zinc-Chromite System. *Journal of the Physical Society of Japan*, 33, 687-.
- Kitaeva, V.F., Zharikov, E.V., and Chisty, I.L. (1985) The properties of crystals with garnet structure. *physica status solidi (a)*, 92, 475–488.
- Kube, C.M. (2016) Elastic anisotropy of crystals. *AIP Advances*, 6, 095209.
- Kube, C.M., and de Jong, M. (2016) Elastic constants of polycrystals with generally anisotropic crystals. *Journal of Applied Physics*, 120, 165105.
- Lafuente, B., Downs, R.T., Yang, H., and Stone, N. (2016) The power of databases: The RRUFF project. In T. Armbruster and R.M. Danisi, Eds., *Highlights in Mineralogical Crystallography* pp. 1–30. De Gruyter, Berlin.
- Ledbetter, H. (2000) Blackman diagrams and elastic-constant systematics. In M. Levy, H. Bass, and R. Stern, Eds., *Handbook of Elastic Properties of Solids, Liquids, and Gases, Vol. II*, pp. 57–64. Academic Press, San Diego.
- Ledbetter, H., and Migliori, A. (2006) A general elastic-anisotropy measure. *Journal of Applied Physics*, 100, 063516.
- (2008) Elastic-constant systematics in f.c.c. metals, including lanthanides–actinides. *physica status solidi (b)*, 245, 44–49.
- Lethbridge, Z.A.D., Walton, R.I., Marmier, A.S.H., Smith, C.W., and Evans, K.E. (2010) Elastic anisotropy and extreme Poisson's ratios in single crystals. *Acta Materialia*, 58, 6444–6451.
- Li, B., and Liebermann, R.C. (2014) Study of the Earth's interior using measurements of sound velocities in minerals by ultrasonic interferometry. *Physics of the Earth and Planetary Interiors*, 233, 135–153.

- Mainprice, D. (1990) A FORTRAN program to calculate seismic anisotropy from the lattice preferred orientation of minerals. *Computers & Geosciences*, 16, 385–393.
- Mainprice, D. (2015) Seismic anisotropy of the deep Earth from a mineral and rock physics perspective. In G. Schubert, Ed., *Treatise on Geophysics (Second Edition)* pp. 487–538. Elsevier, Oxford.
- Mainprice, D., Hielscher, R., and Schaeben, H. (2011) Calculating anisotropic physical properties from texture data using the MTEX open-source package. Geological Society, London, Special Publications, 360, 175–192.
- Marmier, A., Lethbridge, Z.A.D., Walton, R.I., Smith, C.W., Parker, S.C., and Evans, K.E. (2010) EIAM: A computer program for the analysis and representation of anisotropic elastic properties. *Computer Physics Communications*, 181, 2102–2115.
- Muñoz-Santiburcio, D., and Hernández-Laguna, A. (2017) AWESoMe 1.1: A code for the calculation of phase and group velocities of acoustic waves in homogeneous solids. *Computer Physics Communications*, 217, 212–214.
- Nestola, F., Periotto, B., Anzolini, C., Andreozzi, G.B., Woodland, A.B., Lenaz, D., Alvaro, M., and Princivalle, F. (2015) Equation of state of hercynite, FeAl_2O_4 , and high-pressure systematics of Mg-Fe-Cr-Al spinels. *Mineralogical Magazine*, 79, 285–294.
- Niu, H., Chen, X.-Q., Liu, P., Xing, W., Cheng, X., Li, D., and Li, Y. (2012) Extra-electron induced covalent strengthening and generalization of intrinsic ductile-to-brittle criterion. *Scientific Reports*, 2, srep00718.
- Nye, J.F. (1985) *Physical Properties of Crystals: Their Representation by Tensors and Matrices*, 356 p. Oxford U. Press, Oxford, UK.
- Paszkievicz, T., and Wolski, S. (2007) Anisotropic properties of mechanical characteristics and auxeticity of cubic crystalline media. *physica status solidi (b)*, 244, 966–977.
- Pettifor, D.G. (1992) Theoretical predictions of structure and related properties of intermetallics. *Materials Science and Technology*, 8, 345–349.
- Ranganathan, S.I., and Ostoja-Starzewski, M. (2008) Universal elastic anisotropy index. *Physical Review Letters*, 101, 055504.
- Råsander, M., and Moram, M.A. (2015) On the accuracy of commonly used density functional approximations in determining the elastic constants of insulators and semiconductors. *The Journal of Chemical Physics*, 143, 144104.
- Reichmann, H.J., Jacobsen, S.D., and Ballaran, T.B. (2013) Elasticity of franklinite and trends for transition-metal oxide spinels. *American Mineralogist*, 98, 601–608.
- Rieder, M. (2016) The mineralogical system: Can global plots teach us something new? *Mineralogical Magazine*, 80, 239–248.

- Schreuer, J., and Haussühl, S. (2005a) Elastic and piezoelectric properties of minerals I. Principles and experimental approaches. *Mineral Behaviour at Extreme Conditions*, 7, 95–116.
- (2005b) Elastic and piezoelectric properties of minerals II. Structure property relationships. *Mineral Behaviour at Extreme Conditions*, 7, 173–198.
- Simmons, G., and Wang, H. (1971) *Single-Crystal Elastic Constants and Aggregate Properties: A Handbook*. MIT Press, Cambridge, MA.
- Sirdeshmukh, D.B., and Subhadra, K.G. (2005) Consistency checks on elastic properties of crystals. *Journal of Materials Science*, 40, 1553–1570.
- Speziale, S., Marquardt, H., and Duffy, T.S. (2014) Brillouin scattering and its application in geosciences. *Rev. Mineral. Geochem.*, 78, 543–603.
- Stixrude, L., and Jeanloz, R. (2015) Constraints on seismic models from other disciplines - constraints from mineral physics on seismological models. In G. Schubert, Ed., *Treatise on Geophysics* pp. 829–852. Elsevier, Oxford.
- Syono, Y., Fukai, Y., and Ishikawa, Y. (1971) Anomalous elastic properties of Fe₂TiO₄. *Journal of the Physical Society of Japan*, 31, 471–476.
- Ting, T.C.T., and Chen, T. (2005) Poisson's ratio for anisotropic elastic materials can have no bounds. *The Quarterly Journal of Mechanics and Applied Mathematics*, 58, 73–82.
- Walker, A.M., and Wookey, J. (2012) MSAT—A new toolkit for the analysis of elastic and seismic anisotropy. *Computers & Geosciences*, 49, 81–90.
- Wang, H., and Simmons, G. (1972) Elasticity of some mantle crystal structures: 1. Pleonaste and hercynite spinel. *Journal of Geophysical Research*, 77, 4379–4392.
- Wang, X.F., Jones, T.E., Li, W., and Zhou, Y.C. (2012) Extreme Poisson's ratios and their electronic origin in B2 CsCl-type AB intermetallic compounds. *Physical Review B*, 85, 134108.
- Wang, Z., and Ji, S. (2001) Elasticity of six polycrystalline silicate garnets at pressure up to 3.0 GPa. *American Mineralogist*, 86, 1209–1218.
- Watt, J.P. (1988) Elastic properties of polycrystalline minerals: Comparison of theory and experiment. *Physics and Chemistry of Minerals*, 15, 579–587.
- Watt, J.P., Davies, G.F., and O'Connell, R. (1976) Elastic properties of composite materials. *Reviews of Geophysics*, 14, 541–563.
- Weidner, D., Swyler, K., and Carleton, H. (1975) Elasticity of microcrystals. *Geophysical Research Letters*, 2, 189–192.

- Weidner, D.J., Bass, J.D., and Vaughan, M.T. (1982) The effect of crystal structure and composition on elastic properties of silicates. In S.I. Akimoto and M.H. Manghnani, Eds., *High-Pressure Research: Applications in Geophysics* pp. 125–133. Center for Academic Publishing, Tokyo.
- Whitfield, C., Brody, E., and Bassett, W. (1976) Elastic-moduli of NaCl by Brillouin-scattering at high-pressure in a diamond anvil cell. *Review of Scientific Instruments*, 47, 942–947.
- Xiong, Z., Liu, X., Shieh, S.R., Wang, F., Wu, X., Hong, X., and Shi, Y. (2014) Equation of state of a synthetic ulvöspinel, $(\text{Fe}_{1.94}\text{Ti}_{0.03})\text{Ti}_{1.00}\text{O}_{4.00}$, at ambient temperature. *Physics and Chemistry of Minerals*, 42, 171–177.
- Yamanaka, T., Mine, T., Asogawa, S., and Nakamoto, Y. (2009) Jahn-Teller transition of Fe_2TiO_4 observed by maximum entropy method at high pressure and low temperature. *Physical Review B*, 80, 134120.
- Yeganeh-Haeri, A., Weidner, D.J., and Parise, J.B. (1992) Elasticity of alpha-cristobalite: A silicon dioxide with a negative Poisson's ratio. *Science (New York, N.Y.)*, 257, 650–652.
- Zener, C. (1948) *Elasticity and Anelasticity of Metals*, 170 p. University of Chicago Press, Chicago.

Figure Captions

Figure 1. Blackman plot of dimensionless elastic moduli for cubic minerals. The blue dashed lines emanating from the upper left of the diagram are the Zener anisotropy ratios with the heavier blue line indicating the condition for elastic isotropy ($A^Z=1$). The curved red dashed lines show aggregate Poisson ratio values (as indicated by red numbers on the right hand side). The left and upper axes define two of the Born stability criteria ($C_{11}>C_{12}$ and $C_{44}>0$). The black dashed line defines the Cauchy relationship ($C_{12}=C_{44}$) and the green line is given by the relationship: $3C_{11} = 2(C_{12}+2C_{44})$ (Eqn. 30). The solid red line defines the condition for which the Poisson's ratio for $\nu(110, 1\bar{1}0)$ is zero ($3K = A^Z C_{11}$). That is, compositions to the right of the red light are partially auxetic with $\nu(110, 1\bar{1}0)$ less than zero. Structure types and Nickel-Strunz class are indicated in the legend at the right. Diamond is shown by the black symbol.

Figure 2. Blackman plot for garnet- and spinel-structured materials. The lines, symbols, and colors are the same as in Figure 1. The solid blue line connects chromite spinel compositions. Abbreviations are: Sil – silicate, Ox – oxide; Spl – spinel, Grt – garnet, Usp – ulvöspinel, Mag – magnetite.

Figure 3. Blackman diagram for garnets. Rare earth oxide garnets (RE-Grt) are shown as squares, silicate garnets as circles, and germanium garnets as triangles. RE-Grts are colored according to the octahedral/tetrahedral cation: pink=Al, gray = Ga, red = Fe. Silicate garnets are colored according to the dominant constituent(s) as follows: green: pyralspite (pryope, almandine, spessartine); dark green: pryope-majorite (Prp-Maj) solid solution; purple: grossular; light purple: hydrogrossular (Hgr); yellow: uvarovite and andradite; orange Na-rich majorite (Na-Maj). Broken lines give values of Poisson's ratio (red), Zener anisotropy (blue), and the Cauchy relation (black). Gray arrows indicate general trend of chemical substitutions for silicate garnets: 1. Mg^{2+} , Fe^{2+} , $Mn^{2+} \leftrightarrow Ca^{2+}$ in the dodecahedral site; 2. $Fe^{3+} \leftrightarrow Al^{3+}$ in octahedral site; 3. $Cr^{3+} \leftrightarrow Al^{3+}$ in octahedral site; 4. $4H^+ \leftrightarrow Si^{4+}$ in tetrahedral site. Other abbreviations are given in Table 4.

Figure 4. Blackman diagram for binary compounds in the rocksalt (B1), cesium chloride (B2), and sphalerite structures (B3). Lines, symbols, and colors are defined in Figure 1. Solid lines connect compositions in the (Mg, Fe)O solid solution series as well as alkaline earth oxides. Selected phases are identified. X = F, Cl, Rb, I.

Figure 5. Relationship between the ratio of shear to bulk modulus and the Cauchy Pressure ($C_{12}-C_{44}$). Selected individual compositions are identified. Three distinct compositional trends can be

seen in the data as indicated by solid lines. Oxides (light blue) and silicates (red) define one trend while halides (yellow) and sulfides (pink) define a steeper line. A third trend defined by a few materials with a high G/K ratio and strongly negative Cauchy pressure (e.g., diamond, qingsonite, $c\text{-Si}_3\text{N}_4$, SiC) is shown in the inset. Different slopes for these trends reflect differences in the compressibility of these mineral groups. Symbols and colors are the same as in Figure 1.

Figure 6. Distribution of elastic anisotropy among cubic compounds (Eqn. 31). Selected compositions and structural/compositional groups are indicated. The horizontal dashed line at $A^Z=1$ is the value for elastically isotropic materials. Symbols and colors are the same as in Figure 1.

Figure 7. Maximum and minimum Poisson's ratios for strain along $[110]$ for cubic compounds versus degree of elastic anisotropy. One compound lies outside the plotted area: NiCr_2O_4 ($\nu(110, 1\bar{1}0) = -0.78$, $\nu(110, 001)=1.72$, $A^L=4.0$). Symbols and colors are the same as in Figure 1.

Tables

Table 1. Number of compounds with one or more single-crystal elastic modulus measurements for different structure types and different mineral classes.

Class	Garnet	Spinel	Rocksalt	Sphalerite	Fluorite	Perovskite	Pyrite	Other	Total
Silicates	44	8	-	-	-	-	-	4	56
Oxides	21	28	17	-	5	3	-	6	80
Halides	-	-	19	3	5	12	-	4	43
Sulfides	-	1	6	5	-	-	2	-	14
Nitrates	-	-	-	-	-	-	3	-	3
Carbides	-	-	2	1	-	-	-	-	3
Nitrides	-	1	3	1	-	-	-	-	5
Phosphides	-	-	-	1	-	-	-	-	1
Total	65	38	47	11	10	15	5	14	205

One native element (diamond) is also included in the dataset. Germanates (3) are grouped with silicates.

Others are:

Silicates: Zeolite (2), Eulytine (2)

Oxides: Sillenite (3), Bixbyite (2) Cuprite (1)

Halides: Cesium Chloride (4)

Table 2. Percentage of database represented by major structure types.

Structure	% of database
Garnet	31%
Rocksalt	23%
Spinel	18%
Perovskite	7%
Sphalerite	5%
Fluorite	5%

Table 3. Single-crystal elasticity database components.

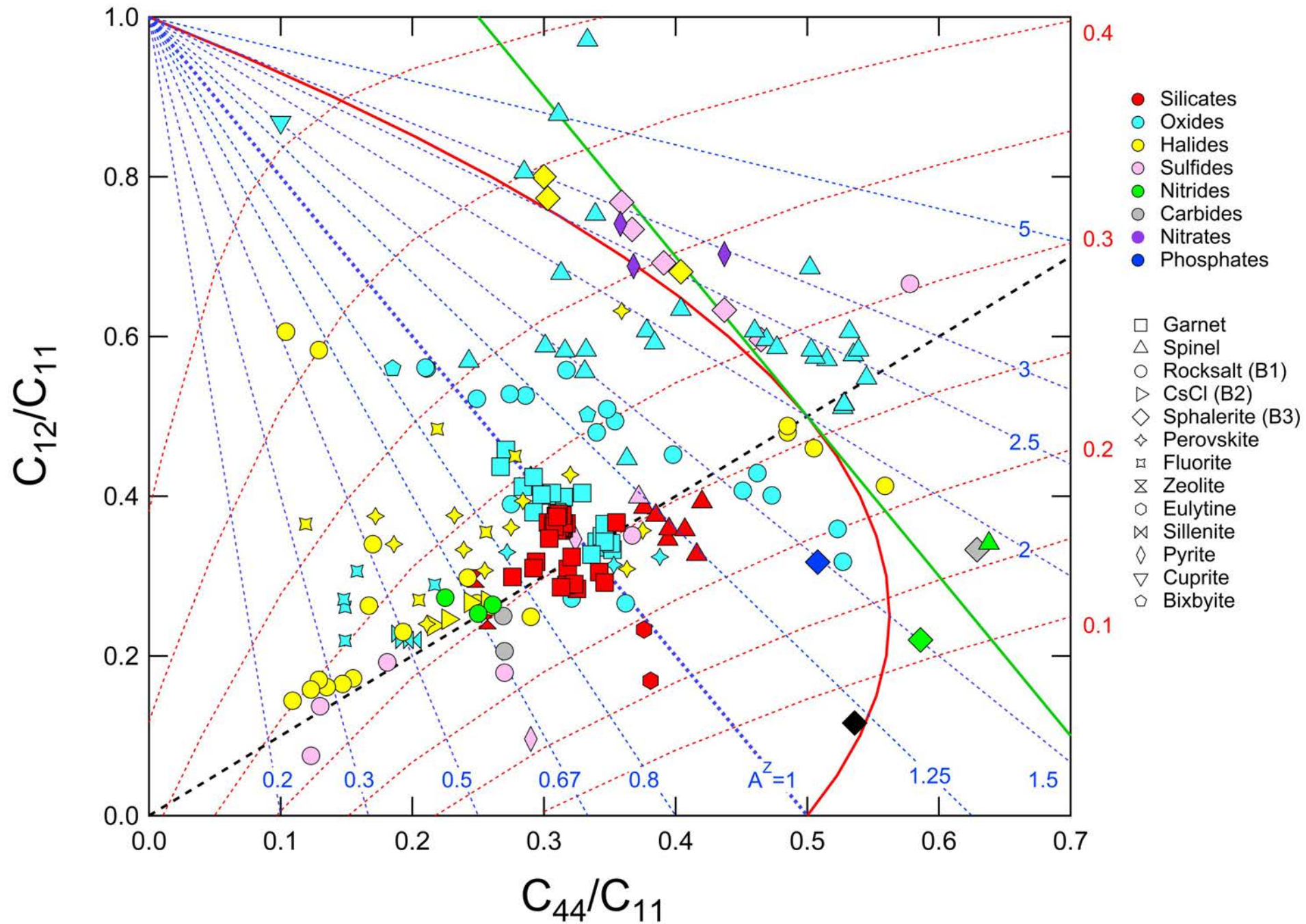
Property	Quantity
Structure and composition	Name, chemical formula, mineral group, structure type, Nickel-Strunz class, density
Adiabatic elastic stiffnesses	C_{11} , C_{44} , C_{12}
Aggregate properties*	Bulk (K) and shear (G) modulus, K/G ratio, Poisson's ratio (ν), Young's modulus (E)
Acoustic properties	Compressional (V_P) bulk (V_B), and shear (V_S) sound velocities, V_P/V_S ratio
Reduced elastic stiffnesses	C_{44}/C_{11} , C_{12}/C_{11}
Anisotropy parameters	Zener (A^Z) Universal (A^U), Kube (A^L), Chung and Buessem (A^G) anisotropy factors
Extrema of Poisson's ratio	$\nu(110,1\bar{1}0)$, $\nu(110,010)$
Adiabatic elastic compliances	S_{11} , S_{44} , S_{12}

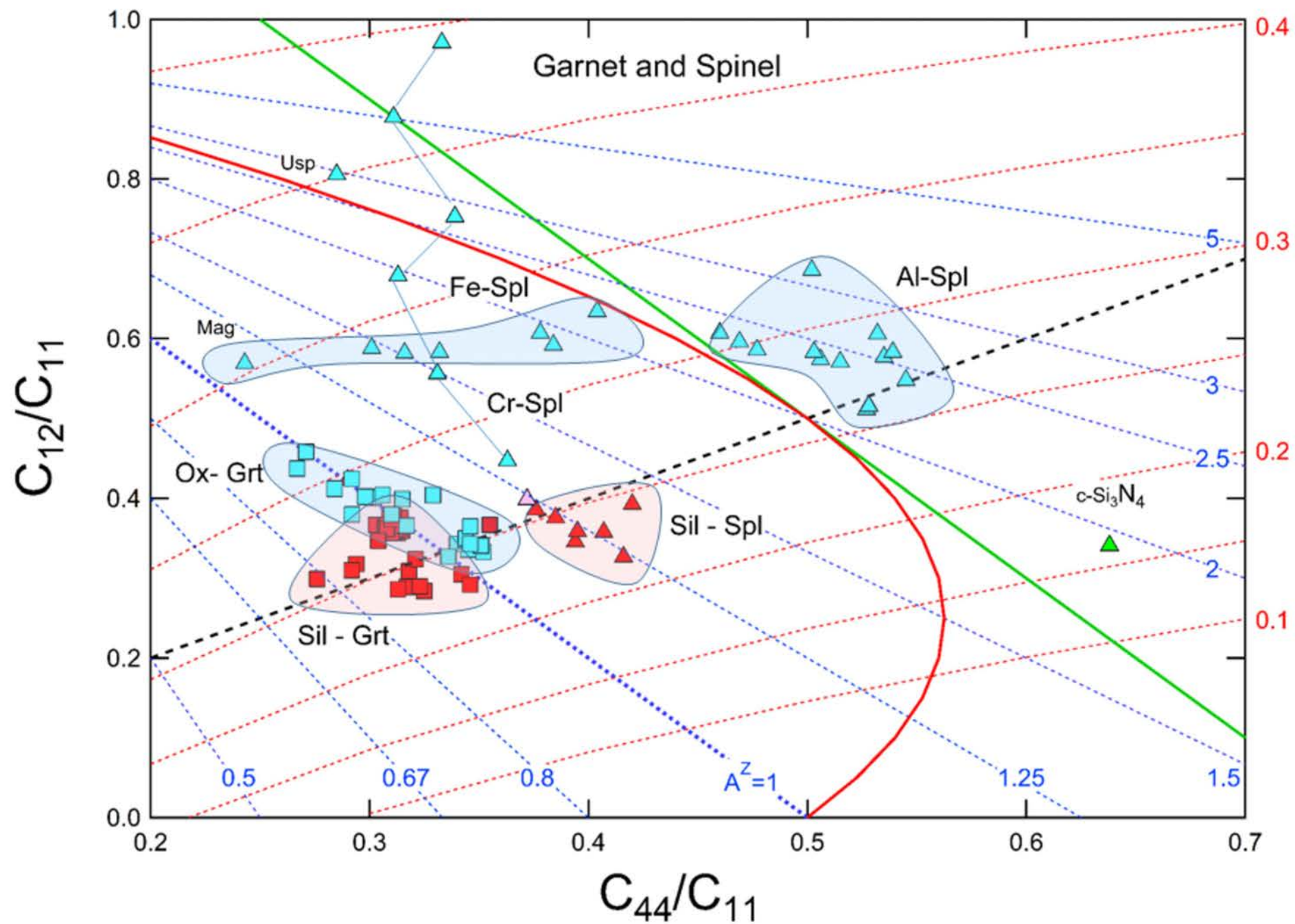
*For shear modulus, compiled values include Voigt, Reuss bounds Voigt-Reuss-Hill average, Hashin-Shtrikman bounds and average; ν and E are obtained from K and VRH average G .

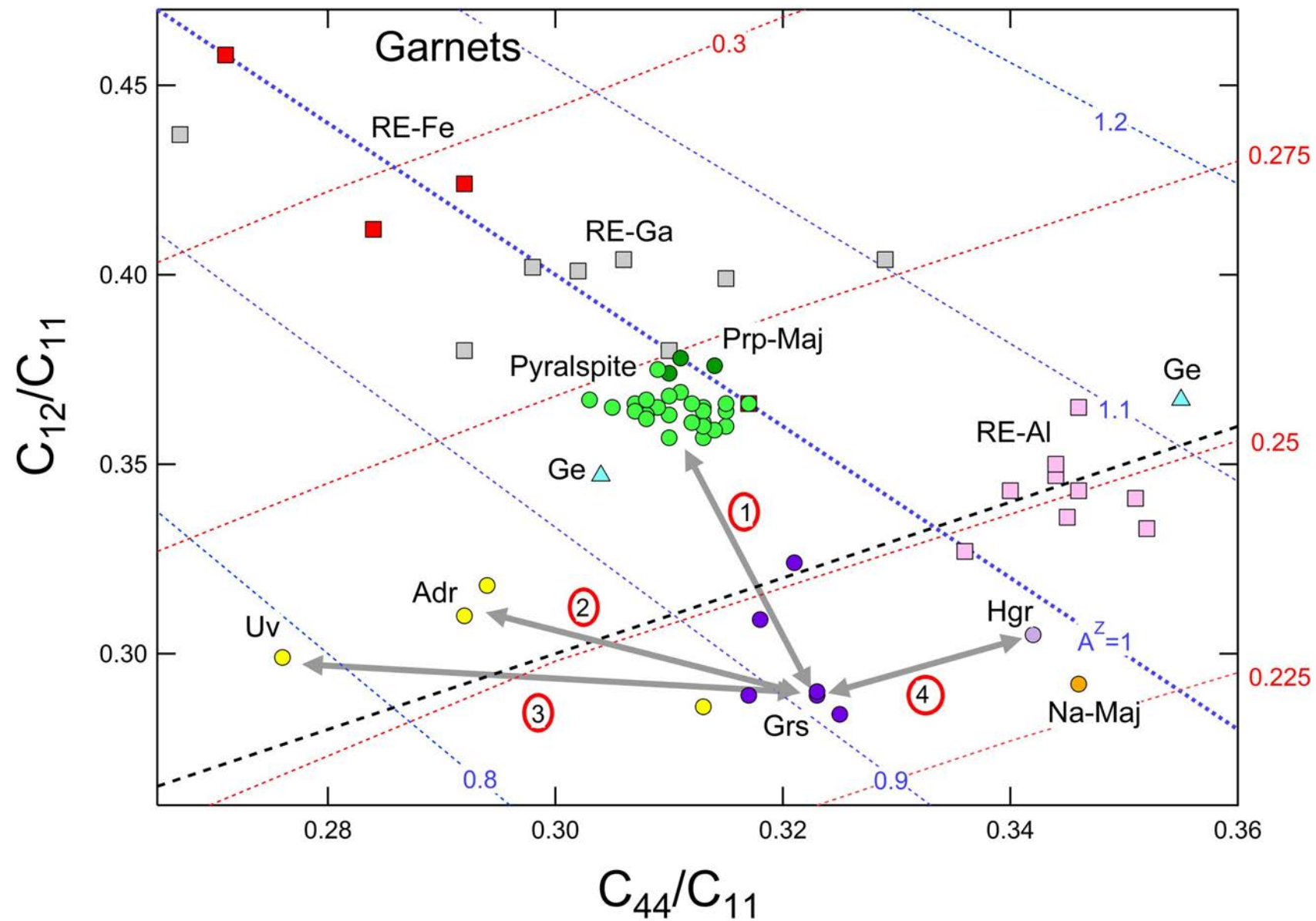
Table 4. Averages of reduced elastic moduli, Zener anisotropy, and Poisson's ratio for garnets subgroups.

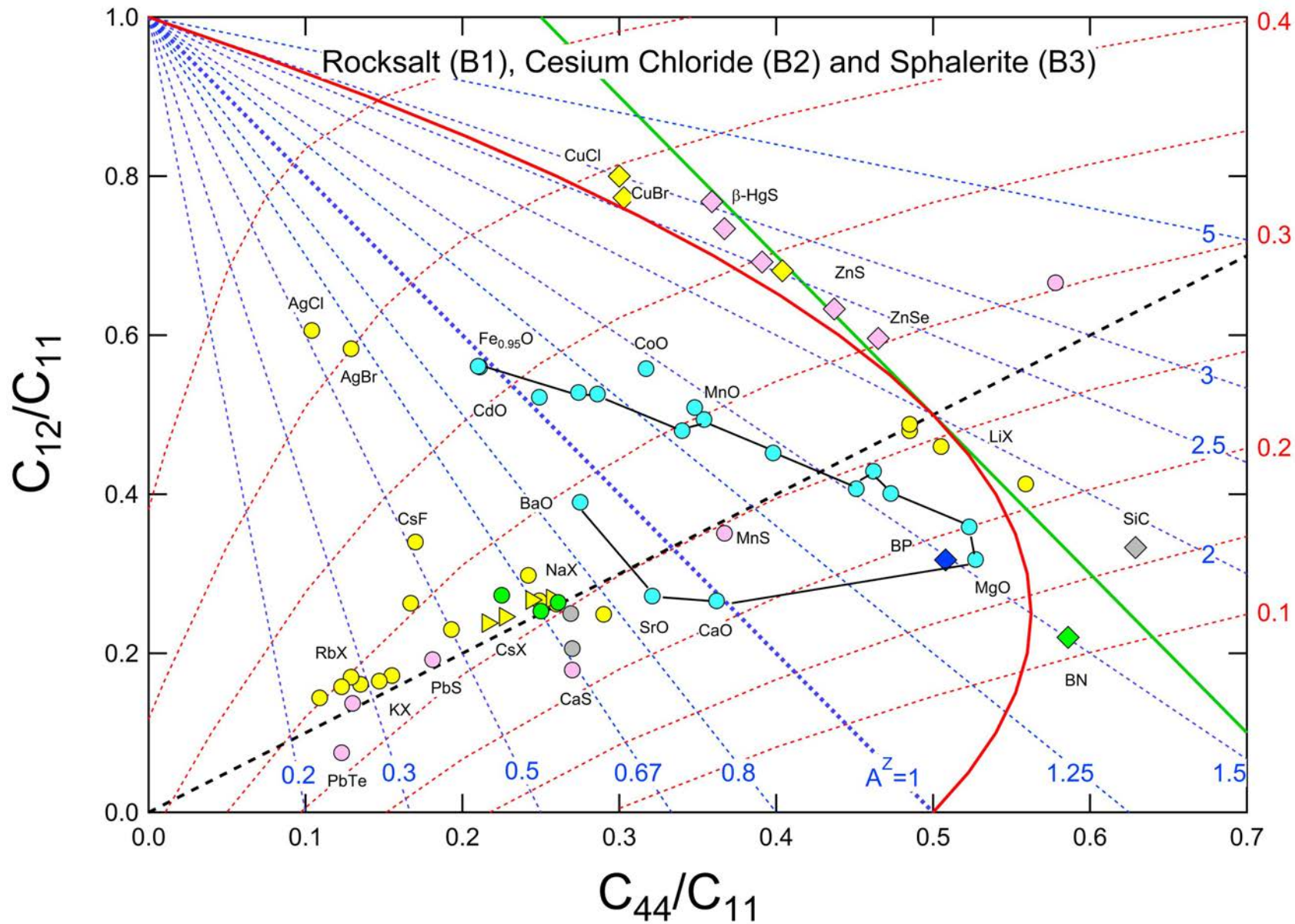
Garnet	#	C_{12}/C_{11}	C_{44}/C_{11}	A^Z	ν
Prp, Alm, Sps	27	0.364(4)	0.311(3)	0.98(1)	0.270(2)
Grs	6	0.296(15)	0.320(4)	0.91(2)	0.241(6)
Adr, Uv	4	0.309(1))	0.287(10)	0.83(3)	0.259(1)
RE-Al	9	0.345(10)	0.346(4)	1.06(2)	0.250(4)
RE-Ga	8	0.398(10)	0.312(11)	1.04(4)	0.280(5)
RE-Fe	4	0.415(38))	0.291(19)	1.00(2)	0.293(19)

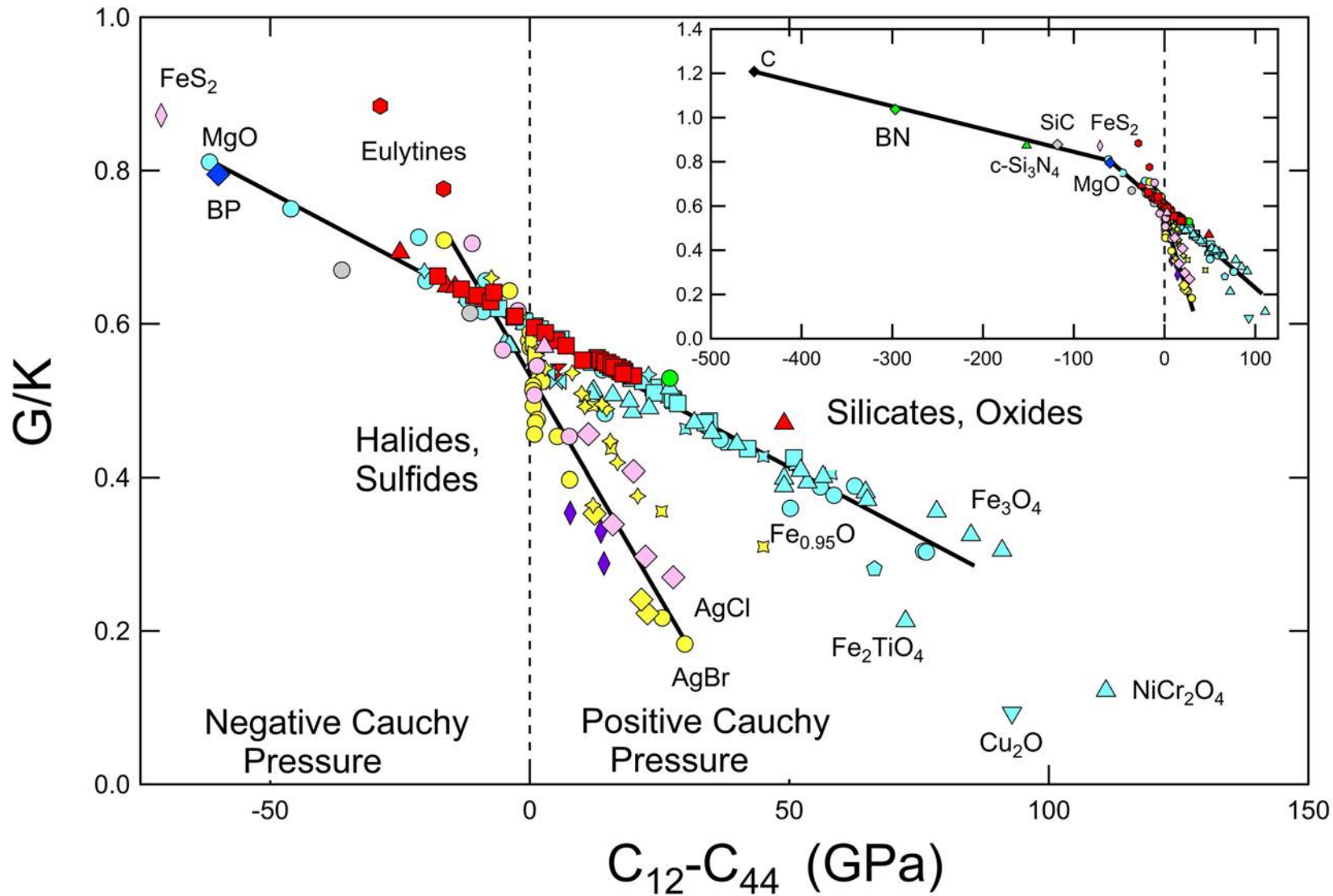
Prp=pyrope, Alm=almandine, Sps=spessartine, Grs=grossular, Adr=andradite, Uv=uvarovite, RE-X =RE₃X₅O₁₂ with X=Al, Ga, or Fe. Number in parentheses is the standard deviation of the mean value.



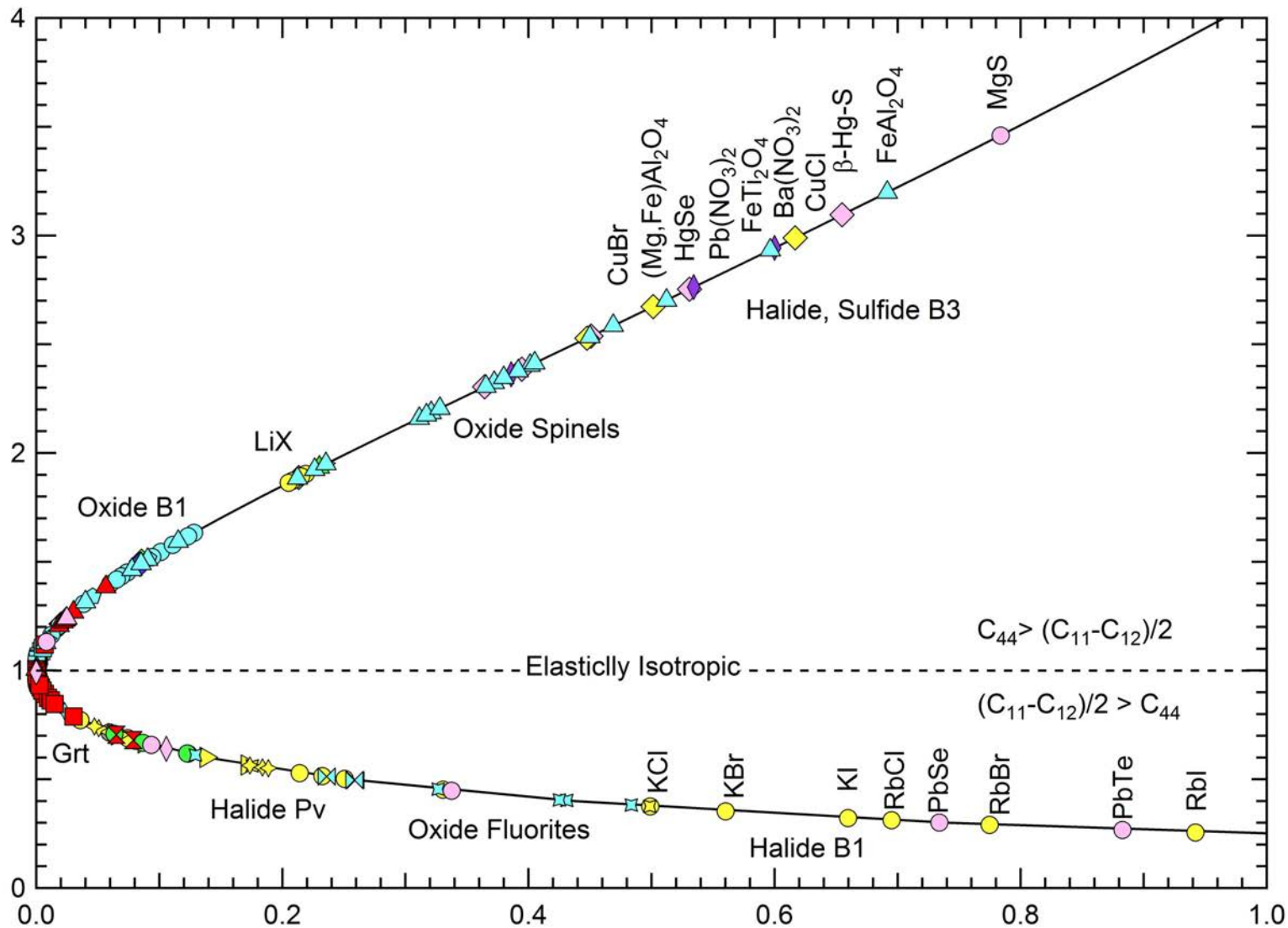








Zener Anisotropy, A^Z



Kube Log-Euclidean Anisotropy Index, A^L

